PAPER

Check for updates

A white-light-emitting single MOF sensor-based array for berberine homologue discrimination†

Qian Wang,[a] Qiao Liu,[a] Xiao-Meng Du,[a] Bo Zhao,[a] Yue Li[*ab] and Wen-Juan Ruan [ID] [*ab]

With multiple signal channels, array sensing can effectively improve detection selectivity, but at the cost of increasingly complex analytical operation and decreased repeatability. Herein, we propose a ''single MOF-based sensor array'' in which a white-light-emitting MOF is used to provide multiple response channels with its manifold emission bands to overcome these drawbacks; the potential of this strategy was verified by the discrimination of berberine homologues (a sub-class of isoquinoline-type alkaloids). A white-light-emitting MOF was synthesized by the incorporation of three luminescent ligands into the UiO-66 backbone. With distinct response behaviors, these components could produce a three-channel signal pattern for the analyte. Thus, this MOF realized array sensing with a single measurement of its spectrum. Its discrimination limit for berberine homologues was as low as 2 μM, and by combination with chemical titration, this MOF could identify samples with unknown concentrations. This work demonstrates the advantage of white-light-emitting MOFs in array sensing.

Introduction

Metal–organic frameworks (MOFs) have attracted great interest as novel fluorescent sensing materials[1–3] By modulation of the aperture and environment of its channels, a MOF can accommodate a specific analyte as a guest and thus selectively respond to it.[4,5] This design principle has achieved great success in the development of MOF sensors for metal ions, nitro explosives and VOCs;[6–8] however, it has met tremendous difficulty in the analysis of more complicated chemicals, such as natural products.[9,10] Because most natural products have vast numbers of homologues, their discrimination is one of the primary challenges in the sensing of these compounds. The homologues usually have similar structures; therefore, they can be equivalently accommodated by MOF channels and thus give undistinguishable signals.

Inspired by mammal olfactory systems, the concept of array sensing may represent an effective way to solve this problem.[11]

Instead of a specific sensor, this technique uses a group of sensing elements to produce a unique response pattern for one analyte. With multiple signal channels, the structural discrimination capability of array sensing is greatly improved.[12–14] A combination of array sensing with MOF fluorescent detection was reported very recently and has already shown great potential. Some difficult tasks, such as the distinction of nitro explosives[15] and the detection of H_2O in D_2O,[16] were achieved by this method. However, in array sensing methods, the responses of a group of sensors must be measured; therefore, the analytical operation and time are multiplied in comparison with single sensor analysis. Moreover, inconsistency of sensor preparation and multiple sets of fluorescence measurements can potentially impair the repeatability of the analysis.

The integration of the functions of sensors, in other words, using a sensor with multiple response channels, is a potential way to overcome these drawbacks. In this way, only a few sensors or even a single sensor must be prepared and measured. This strategy has not yet been applied to MOFs but has been reported with other sensing materials. For example, Yu *et al.* regarded the fluorescence, light scattering and absorption changes of an Au–Ag composite as three signal channels for the discrimination of sulfur species.[17] Hormozi-Nezhad and co-workers used the colorimetric responses of Au nanoparticles at different pH values and salt concentrations to distinguish organophosphate pesticides.[18] However, because the signals were of different types or were obtained under different conditions in these studies, multiple measurements were still needed. Array sensing with a single measurement is still highly desirable.

[a] *College of Chemistry, Nankai University, No. 94 of Weijin Road, Tianjin 300071, China. E-mail: wjruan@nankai.edu.cn, liyue84@nankai.edu.cn*

[b] *Key Laboratory of Advanced Energy Materials Chemistry (Ministry of Education), Nankai University, Tianjin 300071, China*

† Electronic supplementary information (ESI) available: Fluorescent spectra of ligands, PXRD patterns, SEM images and ¹H NMR spectra of all the samples prepared during WLE modulation, effect of TCPP incorporation on MOF channel structure, structure and emission stability of MOF sensor, results of transient fluorescent experiments, comparison among the emission spectra of luminescent components and the absorption spectra of analytes and the calculated spectral integrals, CIE chromaticity diagrams of MOF sensor upon the exposure to berberines, analytical results of berberines mixtures, and raw data of array sensing measurements. See DOI: 10.1039/c9tc05180e

This journal is © The Royal Society of Chemistry 2020

J. Mater. Chem. C, 2020, **8**, 1433–1439 | **1433**

White-light-emitting (WLE) MOFs, an actively investigated sub-class of luminescent MOFs,[19,20] provide a promising candidate to realize this purpose. WLE MOFs present several emission bands with balanced intensities. The change in each emission band can be viewed as a signal channel. Thus, with a single measurement of its fluorescence spectrum, a WLE MOF can provide a set of response data. As a proof-of-concept trial of this strategy, in this work, we synthesized a WLE MOF by the incorporation of three luminescent ligands into the framework of UiO-66. Based on the distinct response behaviors of these components, this MOF produced a unique three-channel signal pattern for each analyte. Five berberine homologues were clearly identified using the MOF.

Experimental section

Materials and characterization techniques

All chemicals were obtained commercially and were used as received without further purification. The aqueous suspensions used in the fluorescence measurements were prepared with ultrapure water.

Powder X-ray diffraction (PXRD) patterns were recorded on a Rigaku D/max-2500 diffractometer with Cu Kα radiation (λ = 0.15406 nm) at 40 kV and 100 mA. Scanning electron microscopy (SEM) images were taken using a JEOL JSM-7500F scanning electron microscope. ^{1}H NMR spectra were collected by a Bruker 400 MHz NMR spectrometer with chemical shifts reported as ppm. Fourier transform infrared (FT-IR) spectra were recorded using a TENSOR Fourier transform infrared spectrometer. N_2 adsorption–desorption experiments were performed using a Micrometrics ASAP 2460 system at 77 K, and the samples were degassed at 80 °C for 5 h before measurement. Steady state fluorescence experiments were carried out on an Agilent G9800A fluorescence spectrometer, and an SPVF-1X0 accessory was used to control the sample temperature at 25 °C. Absorption spectra were taken using a Shimadzu UV-2450 spectrophotometer. Fluorescence lifetimes were measured with an Edinburgh FLS-920 spectrometer.

Synthesis of MOFs

Different molar ratios (1:0, 5:1, 4:1, 3:1, 2:1, 1:1 and 0:1) of 2-aminoterephthalic acid ($H_2BDC-NH_2$) and 2,5-dihydroxyl-terephthalic acid ($H_2BDC-diOH$) with a total amount of 0.15 mmol were dissolved in DMF (5 mL). This solution was placed in a 10 mL Pyrex vial, and $ZrCl_4$ (0.13 mmol), tetra(4-carboxyphenyl)porphyrin (H_4TCPP, 0 to 0.021 mmol) and acetic acid (0.8 mL) were added to it. The mixture was ultrasonicated for 30 min and then heated at 120 °C for 24 h. After cooling to room temperature, the precipitate of the crude product was collected, washed with DMF (6 × 7 mL), solvent-exchanged with methanol (3 × 20 mL) for 24 h and dried in vacuum at 60 °C for 6 h.

Fluorescence sensing

The powder of $TCPP_{0.09} \subset UiO-66-(NH_2)_{0.62}(diOH)_{0.38}$ (5 mg) was immersed in 100 mL water, ultrasonicated for 1.5 h, and then allowed to stand for a day to obtain a stable suspension. In each fluorescence measurement, 3 mL of the suspension was placed in a 1 × 1 cm^2 optical quartz cuvette with continuous stirring at 25 °C in air atmosphere. After the addition of the analyte, the emission spectrum was recorded under excitation at 388 nm (excitation slit = 5 nm, emission slit = 10 nm). Each measurement was repeated five times. The intensity changes at 440, 536 and 645 nm were subjected to linear discriminant analysis (LDA) and hierarchical cluster analysis (HCA) with the Past3 Program (version 3.13).

Analysis of samples with unknown concentrations

The concentration of berberine homologue in the solution was firstly measured by chemical titration.[21] Briefly, 50 mL of the sample was mixed with an aqueous solution of $K_2Cr_2O_7$ (8.3 mM, 5 mL) and stirred for 20 min. After the precipitate was removed by filtration, KI (0.1 g) and hydrochloric acid (6 M, 0.5 mL) were added to the filtrate. The mixture was sealed and placed in the dark for 10 min. The formed I_2 was titrated by $Na_2S_2O_3$ solution (10 mM) with starch as an indicator. Then, with the determined concentration, the berberine homologue sample was added to the MOF suspension to obtain a final concentration of 50 μM. The fluorescence signal of the diluted sample was subjected to LDA analysis and classified by the groups generated through the training matrix with the same concentration.

Results and discussion

WLE MOF construction

Trichromatic (blue, green and red light) and dichromatic (blue and yellow) approaches are two of the most widely used strategies to construct WLE materials.[22,23] We chose the trichromatic strategy because it could provide more response channels. UiO-66 was used as the prototype for the MOF sensor due to its remarkable water stability.[24,25] This MOF was generally functionalized by the mixed-ligand strategy (or ligand replacement). $BDC-NH_2$ and BDC-diOH, which give fluorescent peaks at 428 and 540 nm, respectively (Fig. S1, ESI†), could be incorporated by replacement of the original terephthalate ligand as blue and green emission components. However, by this method, it is difficult to introduce the component with a longer emission wavelength into the UiO-66 framework because the short length requirement to replace the ligand limits the size of its conjugated structure. Recently, Feng and Zhou et al. extended the scope of the mixed-ligand strategy.[26] They found that TCPP, whose geometry is similar, could be integrated as an accessory ligand into UiO-66, and its incorporation amount could be varied in a certain range. The fluorescence measurement of TCPP gave an emission band with a maximum at 645 nm, showing that it can function as a red-emissive component. White light emission could be obtained by the rational modulation of the proportions of $BDC-NH_2$, BDC-diOH and TCPP.

We firstly optimized the ratio of $BDC-NH_2$ to BDC-diOH. In the absence of TCPP, different proportions of these two ligands were reacted with $ZrCl_4$ to obtain a series of MOF samples.
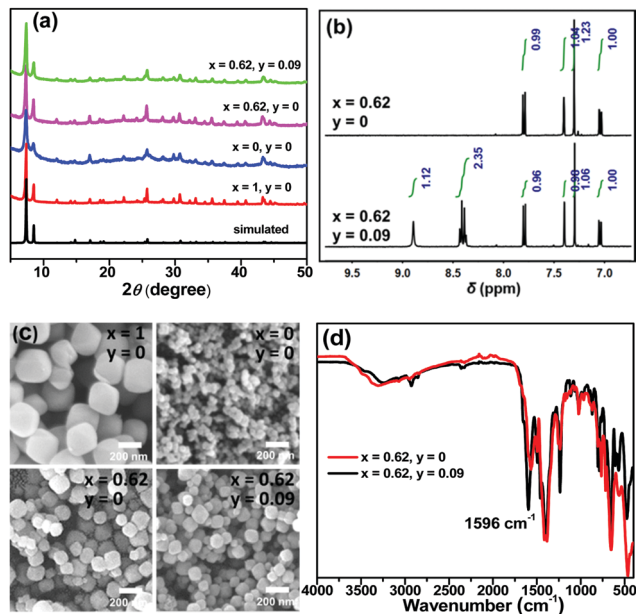
Fig. 1 (a) PXRD patterns, (b) ^{1}H NMR spectra, (c) SEM images and (d) FT-IR spectra of the mainly discussed TCPP$_y$⊂UiO-66-(NH$_2$)$_x$(diOH)$_{1-x}$ samples. The ^{1}H NMR spectra were obtained with solutions of MOFs digested by HF in DMSO-d_6. BDC-NH$_2$ δ: 7.08 (d, J = 8.0 Hz, 1H), 7.42 (s, 1H), 7.78 (d, J = 7.6 Hz, 1H). BDC-diOH δ: 7.30 (s, 2H). TCPP δ: 8.40 (q, 16H), 8.90 (s, 8H).

Fig. 2 Photoluminescence spectra of the suspensions of (a) UiO-66-(NH$_2$)$_x$(diOH)$_{1-x}$ and (b) TCPP$_y$⊂UiO-66-(NH$_2$)$_{0.62}$(diOH)$_{0.38}$. (c) CIE chromaticity diagram for the MOF samples. (d) Photographs of MOF suspensions under UV lamp irradiation. 50 mg L^{-1} MOF in aqueous suspension, λ_{ex} = 388 nm.

PXRD patterns demonstrated the good crystallinity and phase purity of the products (Fig. 1a and Fig. S2a, ESI†). The actual BDC-NH$_2$/BDC-diOH molar ratios in the MOFs were measured by ^{1}H NMR spectra (Fig. 1b and Fig. S3a, ESI†), and according to the results (Table S1, ESI†), these samples are denoted as UiO-66-(NH$_2$)$_x$(diOH)$_{1-x}$ (x = 1, 0.72, 0.69, 0.62, 0.52, 0.37 and 0). SEM observation showed that these samples were composed of octahedron particles with narrow size distributions (Fig. 1c and Fig. S4a, ESI†). With increasing BDC-diOH proportion, the particle size decreased from 200 to 50 nm. The photoluminescence of these samples was directly tested in their aqueous suspensions. As expected, all the mixed-ligand MOFs exhibited dual-emission properties (Fig. 2a). The fluorescent peaks at 428 and 540 nm are characteristic of the BDC-NH$_2$ and BDC-diOH ligands, respectively. The CIE coordinate of the band at 428 nm was calculated to be (0.1540, 0.0564), which is close to the coordinate of (0.14, 0.08) for a saturated blue emitter. In contrast, the 540 nm peak remarkably deviates from the characteristic green emission, and its CIE coordinate falls into the yellow-green region. With decreasing BDC-NH$_2$/BDC-diOH ratio, the fluorescent band at 428 nm weakened, while the emission intensity at 540 nm was enhanced. As a result, the CIE coordinates of the mixed-ligand MOFs were located between the points of UiO-66-NH$_2$ and UiO-66-diOH. Although the emission of BDC-diOH appears at a longer wavelength, its absorption spectrum has no overlap with the emission band of BDC-NH$_2$ (Fig. S5, ESI†); therefore, energy transfer between these two components is impossible. This assumption was further confirmed by transient fluorescence experiments (Fig. S6, ESI†). The emission lifetimes of BDC-NH$_2$ and BDC-diOH in the mixed-ligand MOF (15.71 and 4.77 ns, respectively) were nearly the
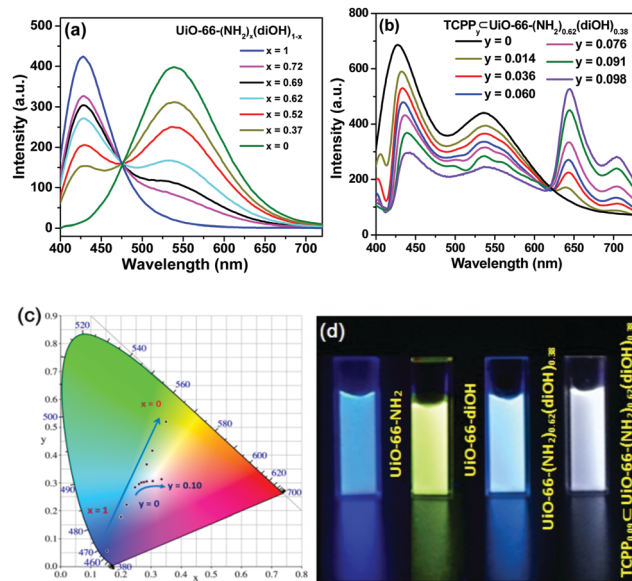
same as those in the samples constructed purely from a single ligand ($\tau_{\text{UiO-66-NH}_2}$ = 15.62 ns; $\tau_{\text{UiO-66-diOH}}$ = 4.68 ns), which indicates that the electronic transitions of these two ligands do not interfere with each other. Based on these results, we attribute the change of emission spectrum with MOF composition to the competition between BDC-NH$_2$ and BDC-diOH for the excitation energy. It was noted that among these samples, UiO-66-(NH$_2$)$_{0.62}$(diOH)$_{0.38}$ presented cyan emission (Fig. 2d), which is complementary to the color red. Its CIE coordinate was also closest to the white light region. Hence, we used this sample as the starting point for TCPP incorporation.

TCPP was incorporated simply by addition of this compound to the synthetic mixture of UiO-66-(NH$_2$)$_{0.62}$(diOH)$_{0.38}$. The incorporation amounts of TCPP were also quantified by ^{1}H NMR spectra, and these samples are labeled as TCPP$_y$⊂UiO-66-(NH$_2$)$_{0.62}$(diOH)$_{0.38}$ (y is the molar ratio of TCPP to the total amount of the original two ligands, Table S1, ESI†). As evidenced by the PXRD patterns, ^{1}H NMR spectra and SEM images, TCPP did not affect the crystallinity, BDC-NH$_2$/BDC-diOH ratio or morphology of UiO-66-(NH$_2$)$_{0.62}$(diOH)$_{0.38}$ when its incorporation amount was lower than 10% (Fig. S2b, S3b and S4b, ESI†). Above this limit, TCPP induced the formation of impurity phase. Because of the low incorporation amount, TCPP caused only a negligible change in the micropore structure of the MOF (Fig. S7, ESI†). In the FT-IR spectrum of the product (Fig. 1d), no peak was shown in the range of 1690 to 1730 cm^{-1}, indicating that the carboxyl groups of TCPP were completely deprotonated and that this component functioned as an accessory ligand. Due to its existence in this form, TCPP exhibited good stability in the MOFs. The immersion of the sample in organic solvents (methanol, acetone and DMSO) or saturated salt solutions

This journal is © The Royal Society of Chemistry 2020

J. Mater. Chem. C, 2020, **8**, 1433–1439 | **1435**

(NaCl, KNO$_3$ and Na$_2$SO$_4$) caused no leakage of TCPP (or the two other ligands) or changes in the crystallinity of the MOFs (Fig. S8, ESI†).

In the photoluminescence spectra, TCPP gave a new emission band with a maximum at 645 nm (Fig. 2b). With increasing TCPP amount, this band was enhanced, while the intensity of the fluorescence from BDC-NH$_2$ and BDC-diOH decreased. We noted that the quenching extent of BDC-NH$_2$ was more remarkable than that of BDC-diOH. Considering the overlap of the emission spectrum of BDC-NH$_2$ with the Soret band of porphyrin (Fig. S5, ESI†) as well as its red-shift after TCPP incorporation, we assume that in addition to competitive absorption, the weakened fluorescence of BDC-NH$_2$ is partly caused by energy transfer to TCPP. This process was proved by the shortened fluorescence lifetime of BDC-NH$_2$ in TCPP$_y$⊂UiO-66-(NH$_2$)$_{0.62}$(diOH)$_{0.38}$ (Fig. S6, ESI†). Then, we calculated the CIE coordinates of the samples. It was observed that when the TCPP amount was increased to 9%, the CIE coordinates shifted to (0.3012, 0.3063), close to the pure white light coordinates of (0.33, 0.33). Therefore, a WLE MOF was obtained through the above modulations (Fig. 2c and d). Composed of three broad bands, the fluorescence spectrum of this MOF covered the whole visible range; therefore, a high color rendering index (CRI) of 91 was obtained. Although dozens of WLE MOFs have been reported to date, most of them were designed by co-doping of Ln ions[27] and embedding of dye molecules.[28] Low CRI and potential leakage of the dye guest are the respective drawbacks of these two types of materials. To the best of our knowledge, before our work, only Telfer's group developed a WLE MOF with pure ligand-centered fluorescence in which the used luminescent ligands were specifically designed.[29] TCPP$_{0.09}$⊂UiO-66-(NH$_2$)$_{0.62}$(diOH)$_{0.38}$ is the second member of this new category of WLE MOFs. Additionally, all three luminescent components of our MOF are commercially available. The facile acquisition of raw materials greatly lowers the cost and simplifies the synthetic procedure of the MOF.

Discrimination of alkaloids

We used TCPP$_{0.09}$⊂UiO-66-(NH$_2$)$_{0.62}$(diOH)$_{0.38}$ to discriminate alkaloids, which are an important class of natural products with extensive applications in traditional and modern medicine. Firstly, arecoline, theophylline, reserpine, quinine and berberine (Scheme 1) were selected respectively as representative derivatives of pyridine, purine, indole, quinolone and isoquinoline, five common types of alkaloids, to roughly test the response of TCPP$_{0.09}$⊂UiO-66-(NH$_2$)$_{0.62}$(diOH)$_{0.38}$. With nanoscale particle size, TCPP$_{0.09}$⊂UiO-66-(NH$_2$)$_{0.62}$(diOH)$_{0.38}$ gave a stable emission in its aqueous suspension after a long measurement time (Fig. S9, ESI†). After the addition of these alkaloids, only berberine caused a remarkable change in the photoluminescent spectrum of TCPP$_{0.09}$⊂UiO-66-(NH$_2$)$_{0.62}$(diOH)$_{0.38}$, and this response was over the full wavelength range (Fig. 3a). Therefore, the following investigation focused on isoquinoline derivatives. To fully demonstrate the structural discrimination capability of the MOF sensor, in addition to berberine, we chose a series of its homologues, including jatrorrhizine, epiberberine, palmatine
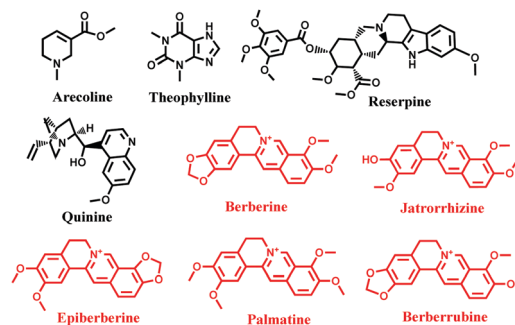
Scheme 1 Structures of the tested alkaloids (the compounds causing fluorescent responses of the MOF are marked in red).
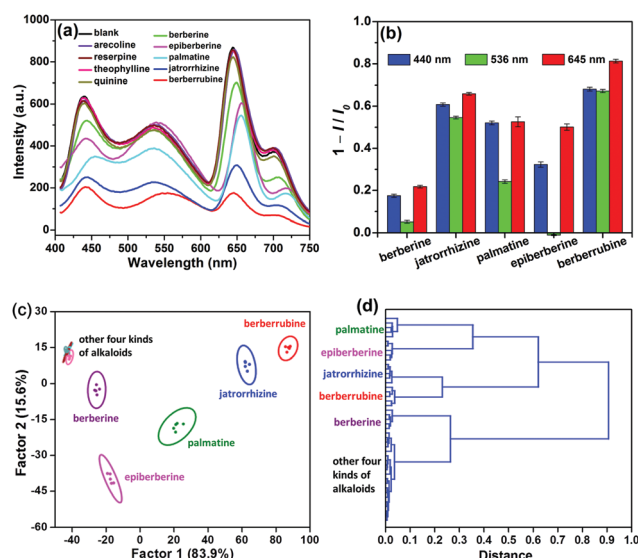

Fig. 3 (a) Fluorescence spectra of TCPP$_{0.09}$⊂UiO-66-(NH$_2$)$_{0.62}$(diOH)$_{0.38}$ (50 mg L^{-1}) after the addition of alkaloids (50 μM). (b) Intensity changes of the three emission bands upon exposure to berberine homologues. (c) LDA and (d) HCA plots for the discrimination of berberines.

and berberrubine, to carry out the sensing experiments. These compounds have the same central conjugated structure; the only difference among them is the substituted methyl/methylene groups on the peripheral O atoms. These compounds could be distinguished if their effects on the three emission bands were different. Upon exposure to the berberine homologues, the quenching efficiencies ($1 - I/I_0$) of the blue band followed the sequence of berberrubine > jatrorrhizine > palmatine > epiberberine > berberine (Fig. 3a and b). This order is consistent with that of the spectral overlap integrals of the absorptions of these chemicals with BDC-NH$_2$ emission (Fig. S10 and Table S2, ESI†), illustrating that the berberine homologues quenched BDC-NH$_2$ by a Förster resonance energy transfer (FRET) mechanism. The shortened fluorescence lifetime of BDC-NH$_2$ in the presence of berberines is in accordance with this mechanism and excludes the radiation energy transfer mechanism (Fig. S11a, ESI†). Because TCPP is excited by energy transfer from BDC-NH$_2$ in TCPP$_{0.09}$⊂UiO-66-(NH$_2$)$_{0.62}$(diOH)$_{0.38}$, the deactivation of the excited state of BDC-NH$_2$ also affects the

1436 | J. Mater. Chem. C, 2020, 8, 1433–1439

This journal is © The Royal Society of Chemistry 2020

emission intensity of TCPP. As a result, the same sensitivity order was shown in the red emission band. However, the intensity change of this band was more prominent, showing that the berberine homologues also affected the energy transfer efficiency from BDC-NH$_2$ to TCPP. The 536 nm band exhibited the lowest sensitivity. Its response order was also different from the blue and red bands; that is, epiberberine, instead of berberine, induced the slightest intensity change in this band. It was noted that the absorption spectrum of epiberberine gave a minimum at 388 nm, which is coincident with the excitation wavelength in the fluorescence experiments. At this wavelength, the absorbances of the five berberine homologues followed the same sequence as their quenching efficiencies on the 536 nm emission band. Therefore, we attribute the response of the green band to an inner filter effect (IFE), which is caused by the competitive absorption of excitation light by the sensor. This mechanism also cannot change the emission kinetics, as verified by transient fluorescence experiments, except for berberrubine (Fig. S11b, ESI†). The slight shortening of the fluorescence lifetime of BDC-diOH by berberrubine indicates that the FRET mechanism also occurs between them, probably because berberrubine has the longest absorption wavelength among the five analytes.

Due to the distinct response behaviors of the three luminescent components of TCPP$_{0.09}$⊂UiO-66-(NH$_2$)$_{0.62}$(diOH)$_{0.38}$, this MOF provides a three-signal fingerprint pattern toward each analyte. The pattern response data obtained above (3 emission bands × 9 alkaloids × 5 replicates, Table S3, ESI†) were firstly treated as the training matrix by linear discriminant analysis (LDA), a supervised statistical technique that aims to project the dataset onto a lower-dimensional space. Three canonical factors, which account for 83.9%, 15.6% and 0.5% of the total variance, were generated from these data. The first two canonical factors were visualized as a 2D score plot, as shown in Fig. 3c. The data points of the five berberine homologues were gathered as five tight clusters with substantial separations between each other. Even the 95% confidence ellipses of these compounds showed no overlap. As a result, the jackknifed classification matrix demonstrated 100% accuracy in the discrimination of all 25 trials of berberine homologues (Table S4, ESI†). The other four alkaloids barely affected the fluorescence of the MOF; therefore, their groups were overlapped and gathered in a small region far from those of the berberine homologues. This result indicates that these compounds cannot interfere with the discrimination of berberines. To further explore the recognition capability of TCPP$_{0.09}$⊂UiO-66-(NH$_2$)$_{0.62}$(diOH)$_{0.38}$, hierarchical cluster analysis (HCA), another supervised differentiating method, was used as an alternative way to treat the raw fluorescence data (Fig. 3d). The five berberine homologues and other unresponsive alkaloids were classified into six different clustering groups, demonstrating the clear distinction of berberines from each other as well as from the interferences.

To estimate the discrimination limit of this "single sensor sensor array", a series of berberine homologue samples with lower concentrations (20, 10, 5 and 2 μM) were measured with it (Fig. S12, ESI†). As shown in the 2D score plots of LDA (Fig. 4), with decreasing analyte concentration, the clusters of the berberine homologues approached each other. In the plot of 2 μM, the 95%
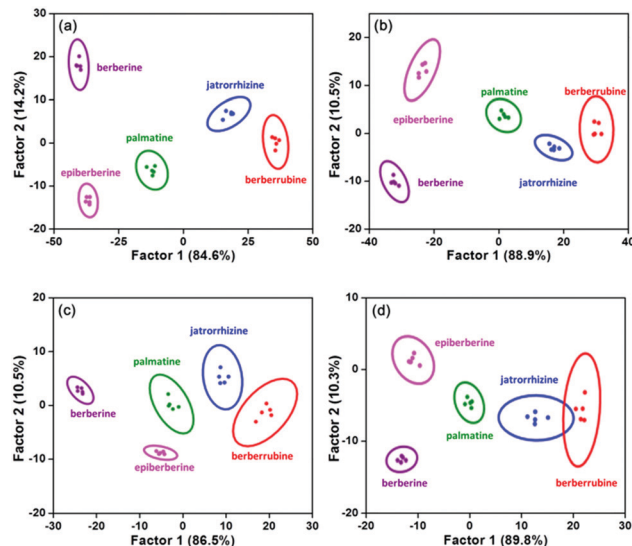

Fig. 4 LDA plots for the discrimination of berberine homologues at (a) 20, (b) 10, (c) 5 and (d) 2 μM with five parallel measurements.

confidence ellipses of jatrorrhizine and berberrubine already showed a large degree of overlap, although the discrimination accuracy of these two compounds was still 100%. Therefore, we conclude that the concentration minimum for the correct classification of berberine homologues is as low as 2 μM. In previous work regarding the multi-target detection ability of WLE MOFs, changes in the emission color were used as the signal to distinguish different analytes.[30,31] Similar to these studies, we also calculated the CIE coordinates of the MOF sensor upon exposure to the berberine homologues. However, even at the analyte concentration of 50 μM (the highest value used in the LDA measurements), the emission color change was still negligible (Fig. S13a, ESI†). This result is not surprising considering that the analyte concentrations and structural differences among the analytes in our work were much smaller than in previous reports. The minimum concentration of berberines to induce a discriminable fluorescence color change was determined to be 200 μM (Fig. S13b, ESI†). The failure of color discrimination proves the necessity to apply the statistical methods of LDA and HCA, which maximize the differences among analyte signals.

The above qualification experiments were carried out with fixed analyte concentrations. However, for most samples encountered in practical analysis, the target concentration is unknown. Therefore, the identification of samples with unknown concentrations is an advanced and more practical challenge. We proposed a procedure of quantification followed by qualification to solve this problem. We noted that, as with berberine, its four homologues also formed precipitates with K$_2$Cr$_2$O$_7$, probably due to their similar structures. This observation indicates that the concentrations of these four compounds can be quantified by the same titration method as berberine. Then, the sample would be diluted to the concentration of the LDA pattern and classified with it. The robustness of this two-step method was examined by blind experiments. Fifteen berberine homologue
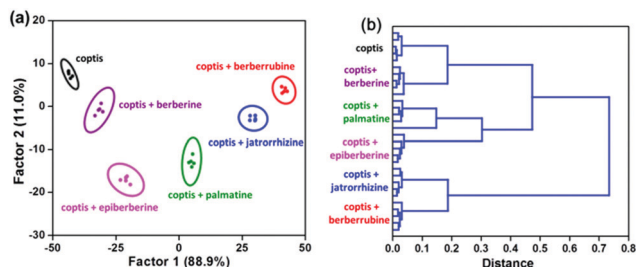
This journal is © The Royal Society of Chemistry 2020

J. Mater. Chem. C, 2020, **8**, 1433–1439 | **1437**

Fig. 5 (a) LDA and (b) HCA plots for $TCPP_{0.09} \subset UiO\text{-}66\text{-}(NH_2)_{0.62}(diOH)_{0.38}$ (50 mg L^{-1}) against berberine homologues (50 μM) in coptidis rhizome extract.

samples (5 analyte × 3 concentration) were randomly prepared as unknowns (both the identity and concentration were blind to the analyzer) and analyzed (Table S5, ESI†). Again, 100% accuracy was obtained in the identification of these samples. This result also confirms that $TCPP_{0.09} \subset UiO\text{-}66\text{-}(NH_2)_{0.62}(diOH)_{0.38}$ can distinguish berberine homologues with a high degree of confidence.

To test the performance of $TCPP_{0.09} \subset UiO\text{-}66\text{-}(NH_2)_{0.62}(diOH)_{0.38}$ in the analysis of complex samples, a series of berberine and berberrubine mixtures with different molar ratios were prepared and measured with it. Each mixture, as well as pure berberine and berberrubine, presented a unique response pattern and could be clearly distinguished in the LDA and HCA plots (Fig. S14, ESI†).

Finally, the potential of this "single sensor sensor array" for practical analysis was evaluated. Because plants are the major producers and sources of alkaloids, the extract of an herb, coptidis rhizome, was used as an example for these experiments. The response of our WLE MOF sensor to coptidis rhizome extract was measured in the absence and presence of berberine homologues (50 μM), respectively. The extract itself and five spiked samples were clearly clustered into six groups by LDA and HCA (Fig. 5), showing that complex plant compositions cannot interfere with analyte identification.

Conclusions

In summary, a trichromatic WLE MOF was prepared by the rational modulation of the proportions of its three luminescent ligands and used in the fluorescence sensing of alkaloids. Even in a single MOF backbone, the three luminescent components exhibited distinct response behaviors; thus, they could be viewed as three sensing elements to construct a sensor array. Five berberine homologues with similar structures were successfully distinguished by this MOF, and the discrimination limit was as low as 2 μM. In combination with chemical titration, this method could even be used to analyze samples with unknown concentrations. Compared with traditional array sensing, this "single MOF sensor array" greatly decreases the analytical operation complexity and time but gives the same amount of information; that is, only one fluorescence spectrum provides sufficient data for analyte identification. This work illustrates the potential of MOFs as an ideal platform to construct multi-responsive sensors.

Conflicts of interest

There are no conflicts to declare.

Acknowledgements

References

1 H. Wang, W. P. Lustig and J. Li, *Chem. Soc. Rev.*, 2018, **47**, 4729–4756.
2 H.-S. Wang, *Coord. Chem. Rev.*, 2017, **349**, 139–155.
3 B. Yan, *Acc. Chem. Res.*, 2017, **50**, 2789–2798.
4 R. Goswami, S. C. Mandal, B. Pathak and S. Neogi, *ACS Appl. Mater. Interfaces*, 2019, **11**, 9042–9053.
5 B. Wang, X. L. Lv, D. Feng, L. H. Xie, J. Zhang, M. Li, Y. Xie, J. R. Li and H. C. Zhou, *J. Am. Chem. Soc.*, 2016, **138**, 6204–6216.
6 H.-R. Fu, L.-B. Yan, N.-T. Wu, L.-F. Ma and S.-Q. Zang, *J. Mater. Chem. A*, 2018, **6**, 9183–9191.
7 D.-M. Chen, N.-N. Zhang, C.-S. Liu and M. Du, *J. Mater. Chem. C*, 2017, **5**, 2311–2317.
8 J. Chen, H. Chen, T. Wang, J. Li, J. Wang and X. Lu, *Anal. Chem.*, 2019, **91**, 4331–4336.
9 Z. Hu, W. P. Lustig, J. Zhang, C. Zheng, H. Wang, S. J. Teat, Q. Gong, N. D. Rudd and J. Li, *J. Am. Chem. Soc.*, 2015, **137**, 16209–16215.
10 S. Wu, Y. Lin, J. Liu, W. Shi, G. Yang and P. Cheng, *Adv. Funct. Mater.*, 2018, **28**, 1707169.
11 K. J. Albert, N. S. Lewis, C. L. Schauer, G. A. Sotzing, S. E. Stitzel, T. P. Vaid and D. R. Walt, *Chem. Rev.*, 2000, **100**, 2595–2626.
12 H. Yang, F. Lu, Y. Sun, Z. Yuan and C. Lu, *Anal. Chem.*, 2018, **90**, 12846–12853.
13 Z. Y. Lin, S. F. Xue, Z. H. Chen, X. Y. Han, G. Shi and M. Zhang, *Anal. Chem.*, 2018, **90**, 8248–8253.
14 S. Sun, K. Jiang, S. Qian, Y. Wang and H. Lin, *Anal. Chem.*, 2017, **89**, 5542–5548.
15 M. Jurcic, W. J. Peveler, C. N. Savory, D. K. Bucar, A. J. Kenyon, D. O. Scanlon and I. P. Parkin, *ACS Appl. Mater. Interfaces*, 2019, **11**, 11618–11626.
16 S. G. Dunning, A. J. Nuñez, M. D. Moore, A. Steiner, V. M. Lynch, J. L. Sessler, B. J. Holliday and S. M. Humphrey, *Chem*, 2017, **2**, 579–589.
17 J.-Y. Yang, T. Yang, X.-Y. Wang, Y.-T. Wang, M.-X. Liu, M.-L. Chen, Y.-L. Yu and J.-H. Wang, *Anal. Chem.*, 2019, **91**, 6012–6018.
18 N. Fahimi-Kashani and M. R. Hormozi-Nezhad, *Anal. Chem.*, 2016, **88**, 8099–8106.
19 M. Pan, W. M. Liao, S. Y. Yin, S. S. Sun and C. Y. Su, *Chem. Rev.*, 2018, **118**, 8889–8935.
20 S. Seetha Lekshmi, A. R. Ramya, M. L. P. Reddy and S. Varughese, *J. Photochem. Photobiol., C*, 2017, **33**, 109–131.

1438 | *J. Mater. Chem. C*, 2020, **8**, 1433–1439

This journal is © The Royal Society of Chemistry 2020

21 *Chinese Pharmacopoeia Commission*, China Medical Science Press, China, 2010.

22 C.-Y. Sun, X.-L. Wang, X. Zhang, C. Qin, P. Li, Z.-M. Su, D.-X. Zhu, G.-G. Shan, K.-Z. Shao and H. Wu, *Nat. Commun.*, 2013, **4**, 2717.

23 A. Wang, Y.-L. Hou, F. Kang, F. Lyu, Y. Xiong, W.-C. Chen, C.-S. Lee, Z. Xu, A. L. Rogach, J. Lu and Y. Y. Li, *J. Mater. Chem. C*, 2019, **7**, 2207–2211.

24 X. Liu, N. K. Demir, Z. Wu and K. Li, *J. Am. Chem. Soc.*, 2015, **137**, 6999–7002.

25 K. Leus, T. Bogaerts, J. De Decker, H. Depauw, K. Hendrickx, H. Vrielinck, V. Van Speybroeck and P. Van Der Voort, *Microporous Mesoporous Mater.*, 2016, **226**, 110–116.

26 Y. Sun, L. Sun, D. Feng and H. C. Zhou, *Angew. Chem., Int. Ed.*, 2016, **55**, 6471–6475.

27 X. Y. Wang, X. Yao, Q. Huang, Y. X. Li, G. H. An and G. M. Li, *Anal. Chem.*, 2018, **90**, 6675–6682.

28 W. Chen, Y. Zhuang, L. Wang, Y. Lv, J. Liu, T. L. Zhou and R. J. Xie, *ACS Appl. Mater. Interfaces*, 2018, **10**, 18910–18917.

29 J. Cornelio, T. Y. Zhou, A. Alkas and S. G. Telfer, *J. Am. Chem. Soc.*, 2018, **140**, 15470–15476.

30 H. Zhao, J. Ni, J.-J. Zhang, S.-Q. Liu, Y.-J. Sun, H. Zhou, Y.-Q. Li and C.-Y. Duan, *Chem. Sci.*, 2018, **9**, 2918–2926.

31 Y. M. Wang, Z. R. Yang, L. Xiao and X. B. Yin, *Anal. Chem.*, 2018, **90**, 5758–5763.

This journal is © The Royal Society of Chemistry 2020

J. Mater. Chem. C, 2020, **8**, 1433–1439 | **1439**